Mode-dependent Energy Management of a Dual-Source Active Switched Quasi-Z-Source Inverter for Fuel Cell Hybrid Vehicles

Thang V. Do, *Student Member*, *IEEE*, Mohsen Kandidayeni, *Member, IEEE*, João Pedro F. Trovão, *Senior Member, IEEE,* Loïc Boulon, *Senior Member, IEEE*

***Abstract*— To prolong the fuel cell (FC) lifetime, hybridizing an FC stack with a lithium-ion capacitor (LiC) bank via a new single-stage power converter is promising in FC hybrid electric vehicles (FC-HEVs). This configuration requires efficient management of its FC hydrogen consumption under various driving conditions. Hence, this paper puts forward a mode-dependent energy management strategy (EMS) for the application of an FC-HEV, employing a high-performance active switched quasi-Z-source inverter (HP AS-qZSI) as its powertrain. Firstly, a supervised learning-based driving mode predictor is utilized to anticipate the driving modes of the FC-HEV. A four-mode fuzzy logic controller (FLC) is subsequently designed and optimized offline by an improved differential evolution (IDE) algorithm for each driving mode. Finally, hardware-in-the-loop tests are carried out to validate the performance of the proposed EMS. The experimental results analyses demonstrate the improved performance of the proposed framework, which reduces the FC hydrogen consumption and the standard deviation of the FC current by 12.67% and 21.31%, respectively, under the studied driving cycle.**

***Index Terms*— Fuel-cell hybrid electric vehicle (FC-HEV), Fuzzy logic controller, Improved differential evolution, Mode-dependent energy management strategy.**

ABBREVIATIONS LIST

BAT	Battery	HEV	Hybrid Electric Vehicle
BC	Boost Converter	GaN	Gallium Nitride
DMP	Driving Mode Predictor	IDE	Improved Differential Evolution
DOD	Depth of Discharge	LQR	Linear–quadratic regulator
EMS	Energy Management Strategy	LiC	Lithium-ion Capacitor
FC	Fuel Cell	MF	Membership Function
FLC	Fuzzy Logic Controller	PEMFC	Polymer Electrolyte Membrane Fuel Cell
GMLP	Gridsearch Multilayer Perceptron	SOC	State of Charge
HIL	Hardware-in-loop	SC	Supercapacitor
HP-AS-qZSI	High-performance Active Switched Quasi-Z-source Inverter	VSI	Voltage Source Inverter
HSP	High-specific Power	ZSI	Z-source inverter
HESS	Hybrid Energy Storage Systems	ZSN	Z-source Network

Manuscript submitted October 25, 2023; revised xxx, 2023; accepted xxx, 2023. Date of publication xxx, 2023; date of current version xxx, 2023. This work is supported in part by Grants 950-230672 from Canada Research Chairs Program and in part by Grants RGPIN-2017-05924 and also in part by FCT-Portuguese Foundation for Science and Technology project UIDB/00308/2020.

Thang V. Do is with the Department of Electrical Engineering and Computer Engineering, University of Sherbrooke, Sherbrooke, QC, J1K 2R1, Canada, (e-mail: Thang.Do.Van.Thang@USherbrooke.ca).

Mohsen Kandidayeni is with the electric-Transport, Energy Storage and Conversion Lab (e-TESC), Department of Electrical Engineering and Computer Engineering, University of Sherbrooke, Sherbrooke, QC J1K 2R1, Canada, and also with the Hydrogen Research Institute (IRH), Université du Québec à Trois-Rivières, Trois-Rivières, QC G8Z 4M3, Canada (e-mail: mohsen.kandidayeni@usherbrroke.ca).

João Pedro F. Trovão is with the Department of Electrical Engineering and Computer Engineering, University of Sherbrooke, Sherbrooke, QC, J1K 2R1, Canada, and also with Polytechnic of Coimbra (IPC-ISEC) and INESC Coimbra, Portugal (e-mail: Joao.Trovao@USherbrooke.ca).

Loïc Boulon is with the Hydrogen Research Institute, University of Québec at Trois-Rivières, Trois-Rivières, QC G9A 5H7, Canada, (e-mails: Loic.Boulon@uqtr.ca).

I. INTRODUCTION

Fuel-cell (FC) lifetime extension plays a critical role in the development of fuel-cell hybrid electric vehicles (FC-HEVs) since the FC system possesses the highest cost of an FC-HEV [1], [2]. Integrating high-specific power (HSP) sources which configure hybrid energy storage systems (H-ESSs) via power converters, is a promising solution [3]. Being regarded as the next generation of the HSP sources, LiCs can assist the FC to decrease its degradation caused by sudden changing loads [4]. These capacitors are constituted by hybridizing the anode of lithium-ion batteries (BATs) and the cathode of supercapacitors (SCs). Subsequently, they can preserve the high-power density of the batteries and obtain greater energy density than SCs.

Regarding the powertrain, classical two-stage inverters, composed of a boost converter (BC) and a voltage source inverter (VSI) is usually exploited in FC-HEVs; nevertheless, this results in decreased performance and increased system cost and volume for these vehicles [5]. To tackle the mentioned restrictions of the BC-VSIs, the employment of single-stage power converters based on Z-source inverter (ZSI) topologies in HESSs has come under attention [4]. These topologies operate with decreased voltage/current stresses, lower input current ripples, and higher efficiencies thanks to their shorter duty cycles, compared to the traditional BC-VSIs. Thus, selecting a proper ZSI topology for the FC-HEV can contribute to enhancing its performance and significantly decreasing its system size and cost. To this end, we proposed a framework based on the multi-criteria decision-making approach to rank various ZSI topologies from the worst one to the best one [4]. Consequently, the active switched quasi-Z-source inverter (AS-qZSI) performed a greater trade-off among multiple criteria than others for our three-wheel-based FC-HEV. However, this selected topology is still of large passive component size and volume. To enhance its usage, a novel HP-AS-qZSI based on HESS FC/LiCs was introduced to enhance the performance and reduce the system size and volume for FC-HEVs in our previous work [6]. This converter is realized by adding one

power-switching device and replacing the LiC bank with the regular capacitor into the Z-source network (ZSN) of the traditional AS-qZSI. In [7], it is shown that the usage of the HESS FC/LiC in the HP-AS-qZSI can achieve lower FC degradation for the FC-HEV than in the conventional two-stage inverter. To guarantee the LiC operation as an HSP source in this topology, it is critical to maintain the LiC state of charge (SOC) in its safe operating range. If the LiC SOC is less than its limitation, the LiC will just operate as a regular capacitor in the ZSN. Consequently, the FC system has to deliver its power at quick transient loads. This leads to sudden FC current variations which negatively influence the FC lifetime. Moreover, this would cause an unstable DC-link voltage in this topology since its DC-link is not adjusted by any controller, resulting in the poor control quality of the electric motor. Thus, the adoption of an appropriate EMS would contribute to not only a reduction in the FC hydrogen (H_2) consumption and the FC lifetime enhancement but also maintaining the operation of this new HESS FC/LiC configuration.

A variety of EMSs have been implemented for efficient energy distribution in FC-HEVs. Regardless of the HEV type, the existing EMSs can be categorized into rule-based, optimization-based and learning-based ones. Fuzzy logic control (FLC) [8] and deterministic control [9] represent primary types of rule-based EMSs. These methods are commonly heuristic and result in non-optimal solutions; nonetheless, straightforward to execute in real-time applications. For instance, the effectiveness of the real-time FLC has been already indicated in [8], where it can meet the energy requirement among various ESSs for unknown driving cycles in FC-HEVs. Optimization-based EMSs, on the other hand, are split into global optimal and real-time ones. Dynamic Programming (DP) and Pontryagin's Minimum Principle (PMP) are instances of the global one [10], [11]. The employment of the DP algorithm for the power distribution in the FC-HEV is discussed in [12]. In [11], the PMP is applied to minimize the energy consumption of the BAT for the HEV. These approaches implement the cost function over a predefined driving cycle, which is useful for obtaining the global optimal benchmark. However, they are difficult for real-time operations because of high computational cost and the reliance on the driving cycle. Concerning real-time EMSs, these strategies give sub-optimal choices. In this respect, their cost function is instantaneously carried out by the system variables. The real-time optimization strategies are well documented, namely Equivalent Consumption Minimum Strategy (ECMS) [13], [14] and adaptive PMP [15], [16]. The main drawback of these approaches is high instantaneous computational time; thus, they might require powerful hardware capability to realize in real-time applications.

With the advancement of artificial intelligence, learning-based EMSs are widely utilized for learning optimal behavior control [17], recognizing driving patterns [18], [19], and optimizing rule-based control [20]. The deep Q learning-based EMS is realized for HEVs in [17], where the fuel economy can be approximate to the global optimum. In [18], a driving mode predictor (DMP) based on supervised learning is explored to enhance the performance of the PMP-based EMS in HEVs. As pointed out, the use of information on driving patterns has a significant effect on the EMS performance in HEVs. Moreover, an adaptive FLC using a neural network classifier-based driving pattern recognition in the FC-HEV also leads to a reduction of 8.89% in the hydrogen consumption and 12.23% in the FC current variation, compared to the conventional optimal FLC [21]. In [20], reinforcement learning is investigated to improve the allocation strategy of the BAT SOC for HEVs. The benefits of these approaches are robustness and highly adaptive learning capability without the need for human intervention; nevertheless, they might be hard to execute in real-time due to the large amount of required complex computation.

So far, several rule-based EMSs have been investigated in dual-source ZSI topologies for various applications. Frequency dividing coordinated control strategies are proposed for HESS SC/BAT ZSI and Bq-ZSI to minimize BAT aging for HEVs [22], [23]. Concerning renewable energy applications, a twofold EMS is studied to distribute power for a BAT energy-stored qZSI in [24]. In [25], an FLC-based EMS is employed in a multi-port qZSI. Nonetheless, these strategies might provide poor energy performance since they are not designed by optimization methods or considering driving conditions. To fill this gap, the usage of an online EMS considering driving patterns to enhance the energy performance in the HESS HP-AS-qZSI can be practiced. On the one hand, the utilization of multi-mode strategies enables the system to transition between various operational modes depending on the current driving scenario. This approach ensures an efficient allocation of energy among the fuel cell system, the battery, and additional energy storage systems, thereby optimizing fuel consumption and extending the lifespan of the components. On the other hand, fuzzy logic control is adept at managing the nonlinearities and uncertainties characteristic of the dynamic driving conditions and energy requirements of FCHEVs. It can adjust to variations in vehicle speed, acceleration, road incline, and other environmental factors, facilitating optimal energy management in real time. Fuzzy logic controls are comparatively straightforward to design and implement. They do not necessitate a precise mathematical model of the system, rendering them resilient to fluctuations in the vehicle's dynamics and external conditions. Consequently, the synergy of these two approaches has made significant interest in the field of energy management strategy design.

In light of the above-discussed matters, this paper investigates a mode-dependent EMS, constituted by a DMP and four optimized FLCs for an FC-HEV. This system uses the HESS HP-AS-qZSI as its powertrain consisting of an FC system and a LiC bank. To the best of the authors' knowledge, this work is one of the first attempts to combine both the supervised learning-based DMP and the multi-FLCs in the new HESS FC/LiC configuration of a Z-source inverter topology for an FC-HEV application. Beyond the theoretical study, this paper is performed around a recreational three-wheel FC-HEV, which regularly experiences high dynamics. Thus, the design of a proper EMS can lead to superior energy performance in terms of the hydrogen consumption and lifetime of the ESSs. The

main contributions of this paper are expressed as follows:

- It proposes an online mode-dependent EMS in a novel dual-source Z-source inverter topology to improve the energy performance regarding the FC hydrogen consumption and FC lifetime for an FC-HEV.
- It presents the employment of an IDE algorithm to optimize the membership function (MF) parameters of the FLC-based EMS.

To validate the performed analysis, a power hardware-in-the-loop (HIL) setup is designed for this purpose.

The rest of the paper is structured as follows. Section II carries out the modeling description of the vehicle powertrain. The framework for designing the proposed EMS is presented in Section III. Section IV provides the obtained results and discussion with HIL validations, followed by the conclusion section.

II. Studied Electric Vehicle Powertrain Architecture

A. Configuration and Specification of the three-wheel FC-HEV

The studied EV, as described in Fig. 1, is a three-wheel recreational vehicle (e-TESC-3W platform) from University of Sherbrooke. To decrease its system size and volume and enhance its performance, a HESS FC/LiC configuration employing a novel HP-AS-qZSI was proposed for this vehicle in our previous work [6]. In this topology, the capacitor C_2 of the HP-AS-qZSI was replaced by a LiC bank operating as both a regular capacitor and an HSP source. This enables the LiC to deliver/restore high-frequency powers immediately in acceleration/regenerative braking operations and maintain the operation of the HP-AS-qZSI. To further improve its usage, the LiC bank is repositioned at the capacitor C_1 of the ZSN in this work as presented in Fig. 1. The parameters of the studied vehicle are illustrated in TABLE I.

B. Dual-Source High-Performance Active Switched Quasi-Z-source Inverter and Hardware-in-the-loop Platform

The modified dual-source HP-AS-qZSI based on HESS FC/LiC for the studied 3-wheel FC-HEV is given in Fig. 1. In [6], the LiC current in the HESS HP-AS-qZSI can be greater than the FC current under the fast acceleration operations of this vehicle. The shoot-through of the HESS HP-AS-qZSI is close to zero, thus its ZSN will not operate in this case. Consequently, this topology has turned into an inverter circuit with the FC and LiC in serial connection. This has a serious impact on the FC lifetime due to the starvation phenomenon. To resolve these issues, by adjusting the LiC bank position in the ZSN, the HESS FC/LiC is considered as a parallel connection via the ZSN. The operating principle of this converter can be found in [6]. Regarding the model of the HP-AS-qZSI, it is performed on the OP4510-based FPGA with a very fast time-step by using the discrete circuit model of power-switching devices to capture their fast transients. In this sense, the Pejovic Switch Model is employed to represent the switch model in RT-Lab software from Opal-RT. This model is realized by a conductance connected in parallel with a controlled current source in [26]. To model the GaN switching device, its power device parameters should be variant according to the operating conditions, and its static current-voltage (I-V) characteristics should be paid attention. However, to simplify the evaluation of the proposed EMS, a simple model of the GaN device is used to execute the HP-AS-qZSI in this work. It is carried out by inserting the parasitic capacitances and gate resistances into the accessible MOSFET model from RT-lab software in Fig. 1. For the purpose of this work, a reduced scale HIL set-up is designed to verify the proposed EMS performance as illustrated in Fig. 2. In this setup, the HESS FC/LiC HP-AS-qZSI is executed on the OP4510-based FPGA, and the TMS320F28335-based experimenter kit is utilized to carry out the control algorithm, where the proposed strategy is executed.

Regarding the FC system setup, a Horizon 500-W air-breathing PEMFC coupled to a National Instrument CompactRIO via its controller, is used. The FC controller

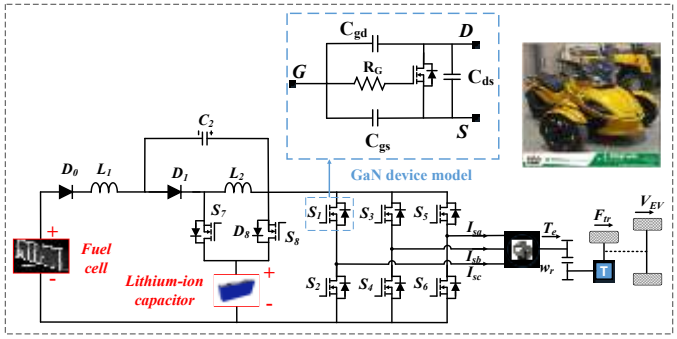

Fig. 1. The proposed configuration of the dual-source HP-AS-qZSI for the e-TESC experimental platform.

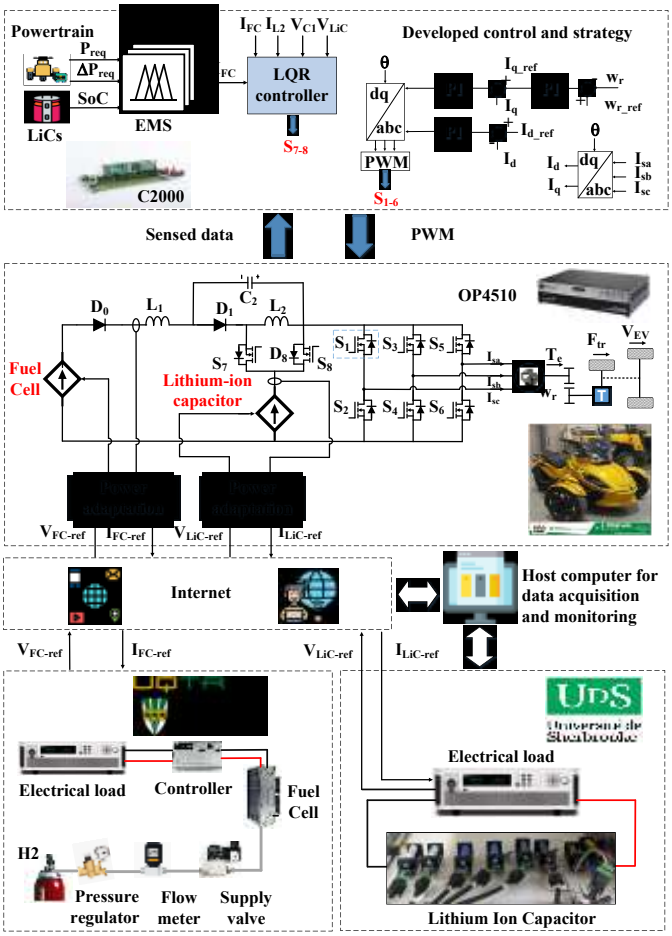

Fig. 2. The experimental setup for HIL simulation.

adjusts the mounted axial fan which is employed for cooling the FC stack and providing the required oxygen. An 8514 BK precision DC electronic load which is connected to the FC controller, is used to represent the obtained FC power profiles from the OP4510. Therefore, this setup allows evaluating not only the used FC model on the OP4510 but also the results of the proposed EMS in a real FC system. According to TABLE I, the three-wheel FCHEV has a 14.4 kW FC system. In this sense, the FC power in Op4510 is scaled down to meet the limited power of the PEMFC in the HIL. To emphasize the significance of the LiC real behavior in the HESS FC/LiC HP-AS-qZSI while designing an EMS, LC0200-380-ASW LiC cells are connected to the DC electronic load (IT6000C Bidirectional Programmable) to figure out their real characteristics.

C. Fuel Cell Model

To estimate the output voltage of the PEMFC, a semi-empirical model investigated by Squadrito *et al.* [27] is applied in this study. This model enables its predicted data to match with the experimental ones over the entire range of the current density with great accuracy. It has only four parameters that need to be tuned, in which they are extracted off-line by using the IDE algorithm. The appropriateness of this steady-state model has been already verified for energy management applications [12]. In this sense, the FC characteristic curve illustrates the relationship between the cell potential (V_o) with the actual current density (J). The FC voltage (V_{FC}) can be determined as follows:

$$V_{FC} = N[V_o - blog(J) - R_{in}J + \alpha J^{\sigma}\ln(1-\beta J)] \quad (1)$$

where N and b show the number of FC cells and the Tafel slope, respectively; R_{in} represents the cell resistance, and α denotes a semi-empirical parameter relating to the diffusion mechanism; σ gives a dimensionless number with respect to the water flooding phenomena; β illustrates the inverse of the limiting current density. The comparison of the predicted and experimental data for the PEMFC is presented in Fig. 3. As is seen, the used FC model can imitate the real FC behavior with high accuracy based on the reported mean square error (MSE).

D. Lithium-ion Capacitor Model

Due to small voltage fluctuations in charging/discharging processes, the LiC operating voltage range (2.2V to 4.2V) is more constant than that of the SC (0V to 2.7V). This enables it to obtain a steadier dc-link voltage in the HP-AS-qZSI and remove the requirement of a pre-charging circuit owing to its greater energy and power density. These merits make it suitable for the HP-AS-qZSI to support the FC system under high-dynamic and fast-changing loads in FC-HEVs. In this paper, the LiC is characterized by a traditional equivalent circuit model, composed of a capacitance element (C_{LiC}) and an equivalent series resistance (R_{LiC}). Its electrical behavior is determined as:

$$u_{LiC}(t) = R_{LiC}i_{LiC}(t) + \int \frac{i_{LiC}(t)dt}{C_{LiC}} + u_{LiC}(t-1) \quad (2)$$

where u_{LiC} and $u_{LiC}(t_0)$ denote the LiC terminal voltage and open circuit voltage, respectively; i_{LiC} illustrates the LiC current.

The LiC capacitance severely relies on its voltage, which can be derived by the modified Stern model of the electrochemical double-layer capacitance.

$$C_{LiC}(v) = \frac{1}{a_H} + \frac{1}{a_1(\frac{e^{a_2\Delta V} + e^{a_3\Delta V}}{2})} \quad (3)$$

$$\Delta V = V_{OCV-LiC} - V_{pzc} \quad (4)$$

where a_H, and $a_{1,2,3}$ are empirical parameters extracted by minimizing the mean square error based on the experimental data. $V_{OCV-LiC}$ expresses the open circuit voltage and V_{pzc} provides the neutral voltage.

The depth of discharge (DoD) of the LiC can be calculated as:

$$DoD(t) = \int \frac{i_{LiC}(t)dt}{3600Q_{LiC}} \quad (5)$$

where Q_{LiC} denotes the amount of the stored charge of the LiC. The relationship between the $V_{OCV-LiC}$ and the DoD can be expressed by a linear function as follows:

$$V_{OCV-LiC}(t) = p_1 DoD(t) + p_2 \quad (6)$$

where p_1 and p_2 are factors that are estimated from the experimental data.

The LiC bank includes a series-parallel combination of LiC cells. Its specifications are presented in TABLE I. Fig. 4 compares the estimation of the LiC output voltage with experimental data. As is noticed, the estimated LiC voltage shows a great agreement with the measured one, indicating the accuracy of the studied LiC model.

TABLE I
FULL-SCALE SYSTEM PARAMETERS

Parameters	Symbols	Values
Vehicles (e-TESC-3W platform)		
Vehicle mass	m_{eq}	350 kg
Vehicle front area	A_{aero}	1.25 m^2
Wheel radius	r	0.305 m
Belt transmission drive ratio	G_{gb}	5.033 (30:151)
Belt transmission drive efficiency	η_{gb}	95%
Maximum vehicle speed	$V_{EV,max}$	140 km/h
PMSM parameters		
Phase inductance	L_d, L_q	62 - 110 µH
Rotor inertia	J	0.096 kg.m^2
Internal phase resistance	R_s	0.0027 Ω
Number of pole pairs	ρ	5
HESS FC/LiC HP-AS-qZSI parameters		
Inductance	$L_{1\text{-}2}$, $L_{BC\text{-}VSI}$	0.2 mH
DC inductor resistance	R_L, $R_{L\text{-}BC\text{-}VSI}$	12.56 - 27.06 mΩ
Capacitance	C_1, $C_{BC\text{-}VSI}$	2.2 – 4.4 mF
Switching frequency	f_s	10 kHz
On resistance	r_{DS}	25.2 mΩ
Internal gate resistance	R_G	0.3 Ω
Input capacitance	C_{ISS}	520 pF
Output capacitance	C_{OSS}	420 pF
Reverse transfer capacitance	C_{RSS}	6.2 pF
Fuel cell parameters		
Number of cell stacks	N_{FC}	75
Rated power	P_{PF}	14.4 kW
Lithium Ion Capacitor parameters for HIL validation		
Operating voltage range	V_{LiCs}	2.2V-4.2V
Neutral voltage	V_{pzc}	3V
Capacitance	C_{LiC}	200 F
Equivalent series resistance	R_{ESR}	45 mΩ
Number of serial cells	$N_{S\text{-}ZSI}$, $N_{S\text{-}BC\text{-}VSI}$	28 - 28
Number of parallel cells	$N_{P\text{-}ZSI}$, $N_{P\text{-}BC\text{-}VSI}$	17 - 17

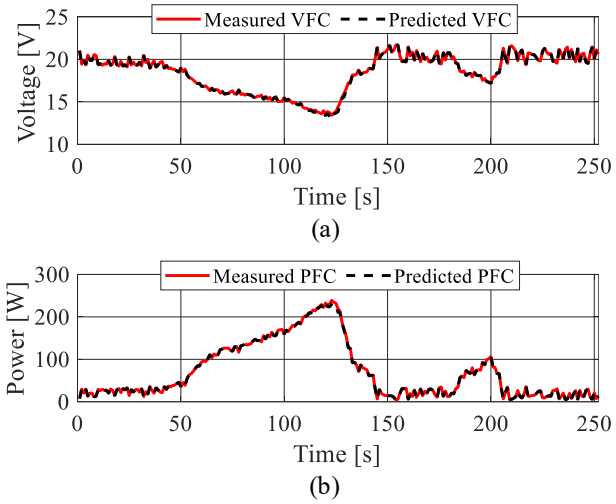

Fig. 3. The predicted FC voltage and power curves, (a) MSE :0.004 and (b) MSE:0.005.

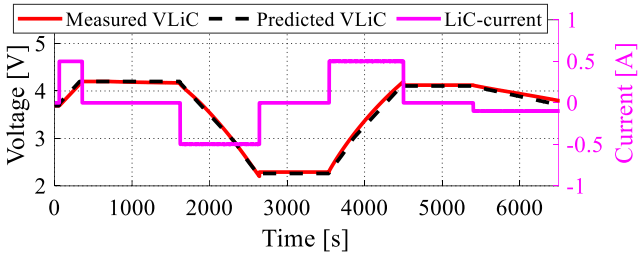

Fig. 4. The predicted LiC voltage curve, MSE :0.028.

III. Proposed Energy Management Strategy

A. Energy Management Strategy Framework

The framework of the suggested EMS is given in Fig. 5. As is observed in this figure, this framework is constituted by three essential parts, namely the IDE-based FLC optimization, driving mode predictor (DMP) and multi-mode FLC. The IDE algorithm is utilized to optimize off-line the MFs of four FLCs by the parts of the WLTC driving cycle. The DMP predicts the driving mode at each sequence and consequently activates the proper FLC-based EMS to fulfill the required FC power in real-time operation. The development of each part is presented in detail hereinafter.

B. Multi-mode Fuzzy Logic Controller

To operate in real-time without prior knowledge of the driving cycle, the proposed mode-dependent EMS should be implemented efficiently to embrace all the driving conditions. In this work, the Gridsearch Multilayer Perceptron (GMLP) classifier-based DMP is applied to figure out the operating mode for the FC-HEV. This DMP is trained by only the WLTC driving cycle, clustered into four driving modes as shown in Fig. 6. Since each cluster possesses a small data volume, this method leads to a less time-consuming optimization process for all the driving data. This makes it suitable to integrate into the proposed strategy. However, this work pays more attention to the proposed framework, and the DMP has been discussed in [18]. Four Mamdani type-based FLCs, specifically FLC Low (FLCL), FLC Medium (FLCM), FLC High (FLCH), and FLC Extra High (FLCEH) according to the operating modes of the vehicle, are adopted to design the proposed mode-dependent EMS. These FLCs are implemented for each driving mode and then integrated to form the suggested strategy. Each FLC is of three inputs, including requested power (P_{req}), the derivation of the requested power (ΔP_{req}), and the LiC SOC. The selection of the ΔP_{req} as an input in these FLCs allows the use of the FC system in a more stable manner. The output of the FLCs is the portion of the P_{req} from the FC system. The inputs are

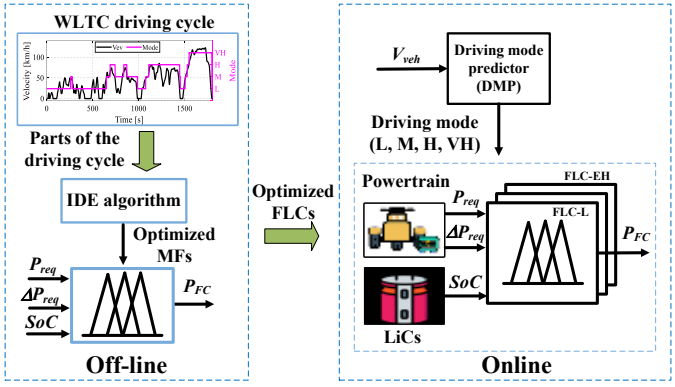

Fig. 5. The framework of the proposed mode-dependent EMS.

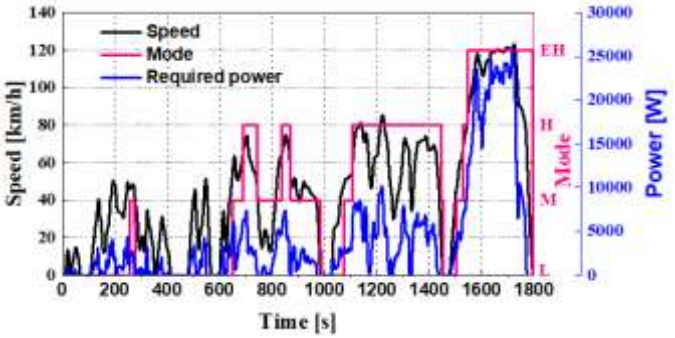

Fig. 6. The WLTC driving cycle and its driving modes.

normalized into the fuzzy domain among 0 and 1 as follows:

$$\begin{cases} Input_1 = \dfrac{P_{req}}{P_{req-max}} \\ Input_2 = \dfrac{SOC_{LiC} - SOC_{LiC-min}}{SOC_{LiC-max} - SOC_{LiC-min}} \\ Input_3 = \dfrac{\Delta P_{req}}{\Delta P_{req-max}} \end{cases} \quad (7)$$

Concerning the rule of the FLCs, they are realized based on the heuristic knowledge of the FC system behavior as illustrated in Fig. 7. In this respect, the input of the FLCs is classified into three fuzzy linguistic domains, such as 'Low' (L), 'Medium' (M) and 'High'(H); their output is represented by 'Very low'(VL), 'Low' (L), 'Medium' (M), 'High' (H) and 'Very high' (VH). These linguistic values are defined by Trapezoidal MFs. Nonetheless, choosing appropriate elements of the MFs has a significant impact on the FLC performance [21]. Traditionally, they are manually tuned, which may not result in optimal choices. In this study, the IDE algorithm is used to figure out the MFs of the four FLCs by using parts of the WLTC, which leads to better FC performance in terms of its lifetime and hydrogen consumption. For instance, the training dataset for determining the MFs of the FLC-L can be derived by combining the required power profiles in the Low modes of

the WLTC from time intervals: [0, 259], [279, 649], [988, 1076], and [1454, 1505] in Fig. 6. In this regard, the required power is achieved by dynamically controlling the FC-HEV operations following to the WLTC, in which this EV model can be developed by using Energetic Macroscopic Representation method as presented in [1]. Moreover, the number of generations and the population size are set to 50, and 100, respectively. The crossover probability and scaling factor are selected randomly from 0.4 to 0.7, and 0.7 to 1, respectively.

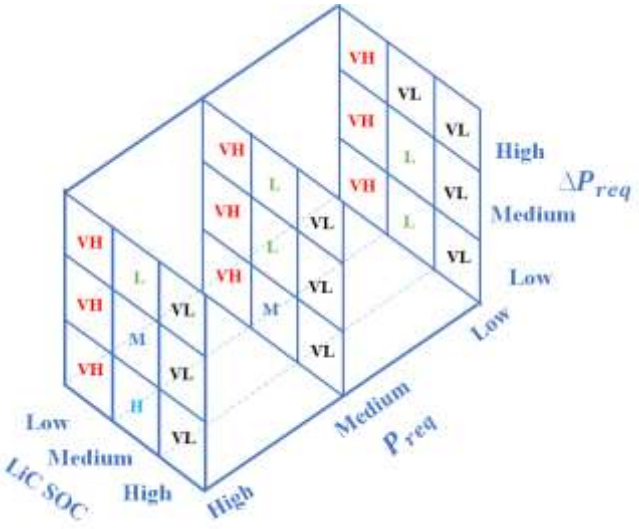

Fig. 7. The designed FLC rule. (Inference mechanism: AND (minimum operator), and defuzzification: centroid).

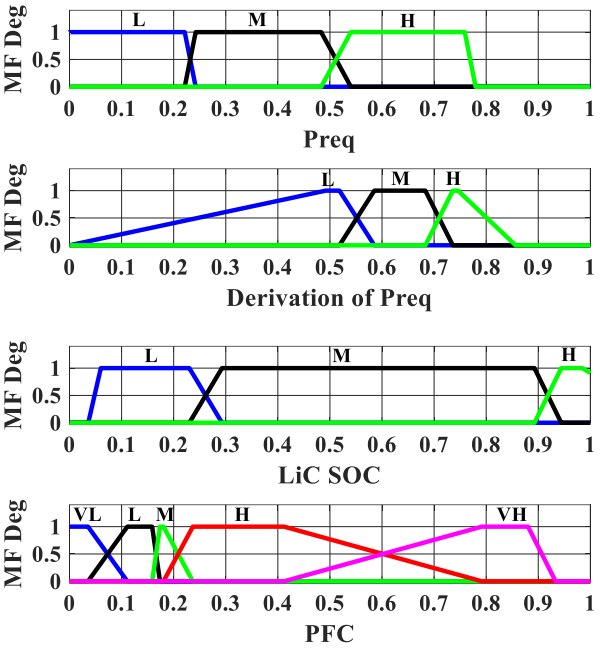

Fig. 8. The MFs of the FLCL.

C. Improved Differential Evolution-based FLC Optimization

To optimize the MFs of the four FLCs, the IDE is carried out by minimizing the objective function in (9). Different from the conventional differential evolution (DE) algorithm, by utilizing multi-mutation operators in the mutation phase, the IDE can perform improved results by efficiently balancing between the global exploration and local exploitation searches. The effectiveness of this improvement has been shown in our previous work [6], where this method illustrates superior performance at optimizing gains of Linear–quadratic regulator (LQR) controllers. Consequently, the IDE-based LQR brings about better dynamic performance for the FC current control than the DE and genetic algorithm (GA)-based LQR. The process flowchart of the proposed IDE-based FLCs in the off-line mode is expressed in Fig. 9. In this flowchart, various sets of MF parameters are first realized by the IDE algorithm. These gains are then employed to simulate the HESS FC/LiC configuration based on their models on Matlab/Simulink. Afterward, the simulation results are used to evaluate the objective function. Once the MF gains of the FLCs are determined, they can be employed in the mode-dependent EMS in an online mode. The procedure of the IDE algorithm is presented as follows:

Initialization: A population with N individuals is randomly produced from the searching space, where each one represents a target vector x_i with V design variables ($i = \overline{1,V}$), derived by:

$$x_{i,j} = x_j^l + rand\,[0,1] \cdot \left(x_j^u - x_j^l\right) \quad (8)$$

where x_j^l and x_j^u illustrate the lower and upper constraints of x_j, respectively.

Objective function: To extend the FC lifetime and reduce the H_2 consumption, weighting factors should be used to convert these two objectives into one objective. However, we consider them as the same priority in this study, thus the following objective function is employed:

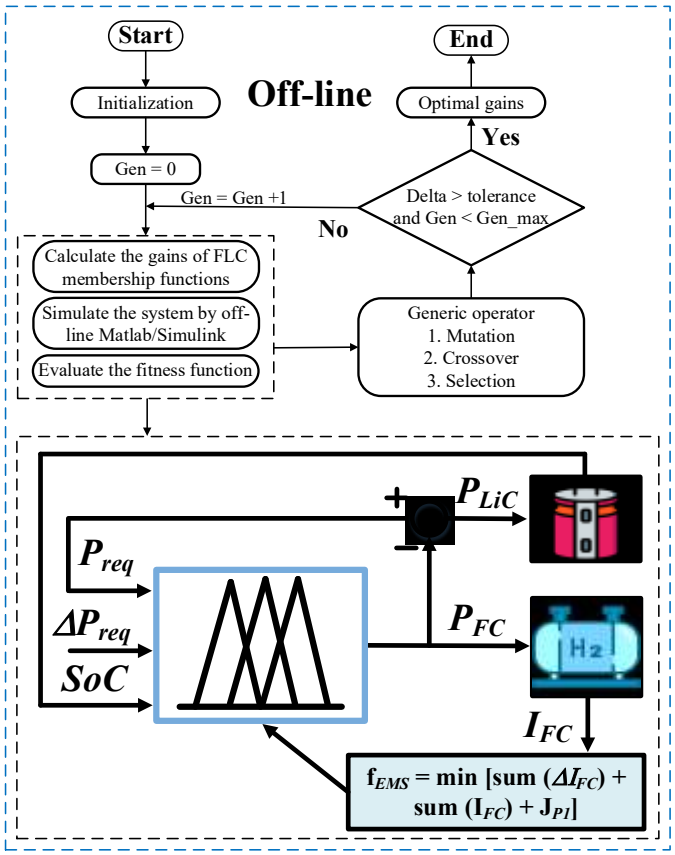

Fig. 9. Process flowchart of optimizing the FLC using the IDE algorithm.

$$f_{EMS} = \int I_{FC}dt + \int |\Delta I_{FC}|dt + J_{p1}$$
$$\text{s.t: } P_{req} = P_{LiC} + P_{FC}$$
$$0 < P_{FC} < 14.4\,\text{kW}$$
$$0 < I_{FC} < 300\,\text{A} \quad (9)$$
$$-5\,kW < \Delta P_{FC} < 5\,kW$$
$$0.3 < SOC_{LiC} < 0.9$$

where $J_{p1} = \begin{cases} 0 & if\ 0.3 \le SoC \le 0.9 \\ 10 \cdot f_{EMS}\ if\ SoC > 0.9\ or\ SoC < 0.3 \end{cases}$ is the penalty factors; ΔI_{FC} shows the derivation of the FC current (I_{FC}).

Mutation: A mutant vector (v_i) is defined by four mutation operators, "rand/1", "rand/2", "best/1" and "best/2", based on each x_i. In this stage, these operators will be adaptively employed during the searching operation:

```
if (delta > threshold)
    if rand [0,1] > 0.3
    Choose aimlessly r1 ≠ r2 ≠ r3 ≠ i, i = 1,N
      rand/1: vi = xr1 + SF ·(xr2 − xr3);
    else
    Choose aimlessly r1 ≠ r2 ≠ r3 ≠ r4 ≠ r5 ≠ i, i = 1,N
      rand/2: vi = xr1 + SF ·(xr2 − xr3) + SF ·(xr4 − xr5);
    end
else (delta <= threshold)
    if rand [0,1] > 0.3;
    Choose aimlessly r1 ≠ r2 ≠ best ≠ i, i = 1,N
      best/1: vi = xbest + SF ·(xr1 − xr2);
    else
    Choose aimlessly r1 ≠ r2 ≠ r3 ≠ r4 ≠ best ≠ i, i = 1,N
      best/2: vi = xbest + SF ·(xr1 − xr2) + SF ·(xr3 − xr4);
    end
end
```

where r_1, r_2, r_3, r_4, and r_5 are randomly selected from $\overline{1,N}$ so that $r_1 \neq r_2 \neq r_3 \neq r_4 \neq r_5 \neq i$; SF shows the scale factor, aimlessly generated in [0.4, 1.0]; x_{best} denotes the best individual in the existing population; and delta is calculated by:

$$delta = abs\left(\frac{f_{mean}}{f_{best}} - 1\right) \quad (10)$$

where f_{best} illustrates the value of the cost function for the best individual; f_{mean} gives the mean one for the whole population.

Crossover: A trial vector u_i is figured out by using a binomial crossover operation as:

$$u_{i,j} = \begin{cases} v_{i,j}\ if\ rand\ [0,1] < CR \\ x_{i,j}\ otherwise \end{cases} \quad (11)$$

where CR gives the crossover control parameter, randomly chosen in the interval [0.7,1].

Selection: To retain good information for the next generation, the selection stage employs the elitist selection method. Firstly, the offspring population O, consisting of all u_i generated from the crossover phase, is merged with the parent population P of the x_i to figure out a mixing population M. The new population is then organized by selecting the N best individuals in M for the upcoming one.

IV. Results and Discussion

To assess the effectiveness of the proposed mode-dependent EMS, a comparative analysis is performed in this section. In this respect, two primary scenarios are taken into consideration. The first one is implemented in offline Matlab/Simulink by simulating only the HESS FC/LiC configuration without power converters. The second one is conducted on the developed HIL setup in Fig. 2 to verify the real-time operation of the proposed EMS in both the HESS HP-AS-qZSI and the HESS conventional BC-VSI for the FC-HEV.

In the first scenario, the performance of the proposed mode-dependent EMS is compared with offline optimized EMSs using the IDE algorithm regarding hydrogen consumption over three driving cycles: FTP, NEDC, and WLTC class 2. In this respect, the FLC-based EMS is figured out by optimizing its MFs based on the whole WLTC driving cycle. By contrast, other EMSs, namely FLCL-based EMS, FLCM-based EMS, FLCH-based EMS, and FLCEH-based EMS are determined by only using parts of the WLTC driving cycle. The 14.4 kW FC system is utilized in this scenario. Fig. 9 indicates the attained simulation results of the proposed EMS for the FTP driving cycle. Fig. 9a shows the speed and predicted driving mode of the vehicle. The requested and HESS powers are presented in Fig. 9b. From these figures, it can be noticed that the FC system is being employed to deliver the average portion of the demanded power, while the LiC is mostly responsible for providing/absorbing the high-frequency energies instantaneously. The comparative analysis results are provided in Fig. 11, where the proposed EMS has achieved a reduced total H_2 consumption over others. Therefore, using a single optimized EMS makes it difficult to allocate energy efficiently under various driving conditions. In the second scenario, to illustrate the capability of the proposed mode-dependent EMS, its performance is firstly assessed in both the HESS HP-AS-qZSI and the semi-active FC/LiC traditional BC-VSI. Then, the FLC-based EMS and rule-based EMS are compared to this proposed strategy in the HESS FC/LiC HP-AS-qZSI. These evaluations are performed under three driving cycles, namely FTP-short, NEDC-short, and WLTC-short. In this regard, the FTP-short driving cycle is realized from time 0s to 340s of the FTP, while the NEDC-short and WLTC-short driving cycles are extracted from their original ones from time 800s to 1200s, and 600s to 1000s, respectively. Moreover, the rule-based EMS is developed by using a six states-based EMS as discussed in our previous work [7]. Fig. 12 indicates the waveforms of the vehicle speed and its predicted mode achieved from the experimental HIL under the FTP-short driving cycle. As is observed, the speed shows a great agreement with its reference under various operating modes of the FC-HEV. Regarding the operation of the proposed EMS in two HESS FC/LiC configurations, it can be realized by waveforms of the FC, LiC, and demanded powers in Fig. 13. According to this figure, the power distributed by the suggested EMS can satisfy the requested powers, and the LiCs frequently discharge their power to decrease the FC stress under the fast transient of the demanded power. Moreover, the HESS HP-AS-qZSI performs a lower FC power than the HESS conventional one. This is mainly because this topology obtains a reduced requested power thanks to its higher efficiency. With respect to the performance of the proposed EMS, the experimental results of the FC, LiC, and requested powers using the FLC-based EMS and the rule-based EMS in the HESS HP-AS-qZSI are given in Fig. 14. Based on Fig. 13a and Fig. 14, the FC power can be

significantly decreased by using the proposed EMS. This contributes to a reduced H_2 consumption over others.

Consequently, the LiC SOC of the suggested one is lower than that of the others since its LiC supports as much as possible power to reduce this consumption in Fig. 15. The comparative results obtained from the experimental HIL over three driving cycles are given in Fig. 16. The total H_2 consumption in two topologies is illustrated in Fig. 16a. As is seen, by using the proposed EMS in these two topologies, the total H_2 consumption of the HESS HP-AS-qZSI is 2.022 g, 1.92 g, and 1.825 g, whereas that of the HESS traditional one is 2.073 g, 2.181 g, and 1.859 g for the FTP-short, NEDC-short, and WLTC class2-short, respectively. These results are primarily due to lower FC current ripples and reduced required powers in

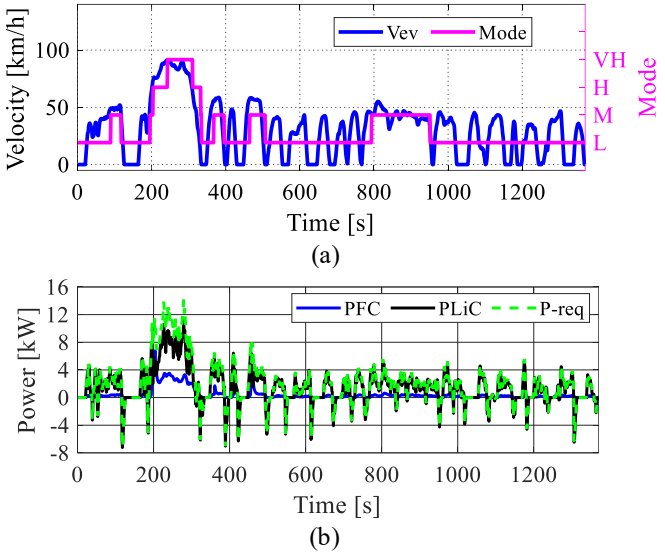

Fig. 10. Simulation results of the vehicle speed and HESS powers, (a) the vehicle speed, (b) the HESS powers.

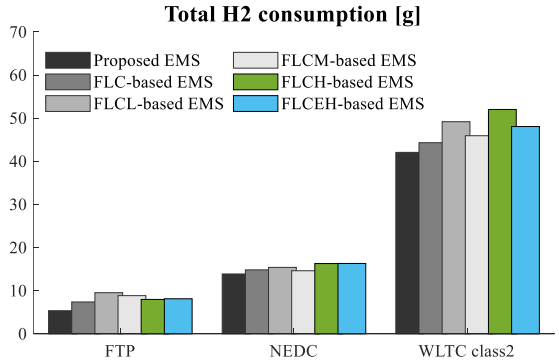

Fig. 11. Simulation results of the total H_2 consumption.

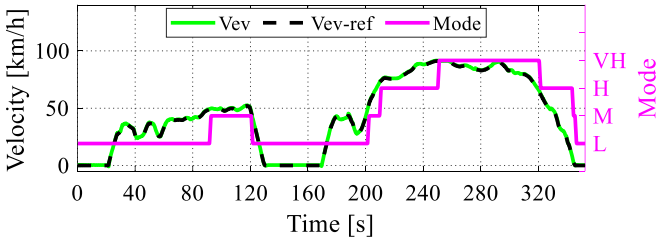

Fig. 12. Experimental results for the vehicle speed and its operating mode.

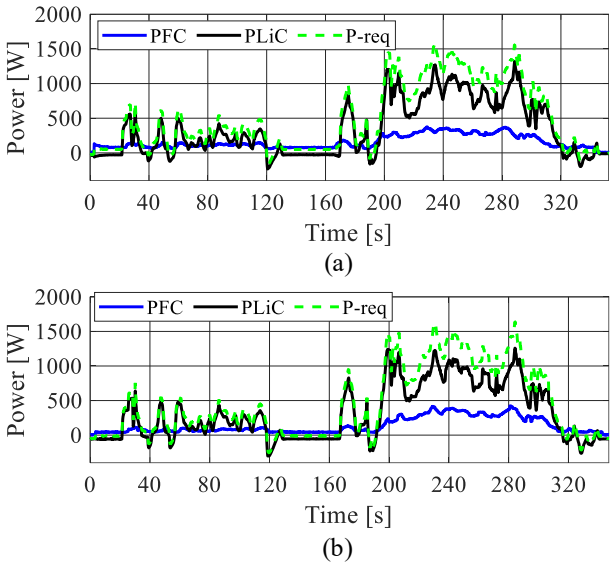

Fig. 13. The experimental waveforms of the HESS powers using the proposed EMS, (a) the HESS HP-AS-qZSI, (b) the HESS BC-VSI.

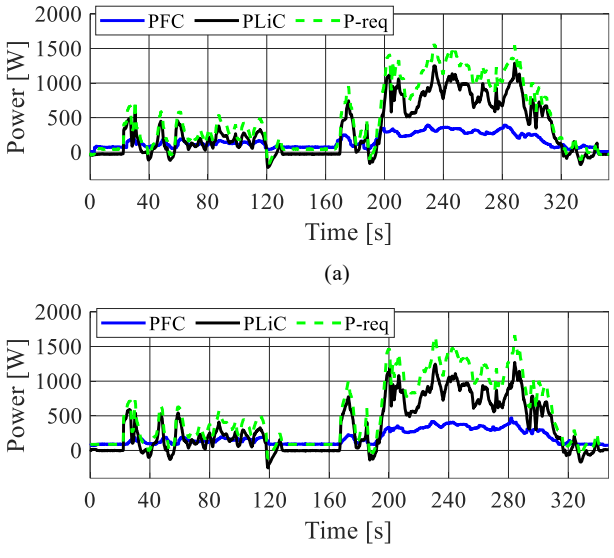

Fig. 14. The experimental waveforms of the HESS powers, (a) the FLC-based EMS, (b) the rule-based EMS.

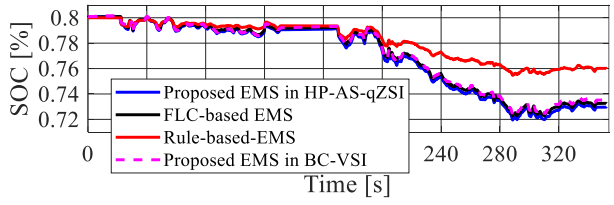

Fig. 15. The experimental results of the LiC SOC.

the HESS HP-AS-qZSI, compared to the HESS BC-VSI. Based on Fig. 16a, the utilization of the proposed strategy in the HESS FC/LiC HP-AS-qZSI leads to a decrease in this consumption by 2.46%, 11.96%, and 1.83%, respectively over the HESS conventional one under the three driving cycles. Compared to the rule-based EMS, the proposed one also allows to reduce remarkably the total H_2 consumption in the HESS HP-AS-qZSI from 12.76% for the FTP-short, 17.09% for the NEDC-short and 14.63% for the WLTC class2-short. The standard deviation

of the FC current can be determined using Fig. 16b. From this figure, the suggested one decreases this result in the HESS FC/LiC HP-AS-qZSI from 21.31% for the FTP-short, 8.01% for the NEDC-short and 27.4% for the WLTC class2-short, compared to the rule-based EMS. Furthermore, its deployment in the HESS FC/LiC HP-AS-qZSI results in reducing this index by 11.57%, 3.89%, and 4.51%, respectively over the conventional HESS one. The above analysis shows that the FC hydrogen consumption and current variation are notably reduced by employing the proposed mode-dependent EMS.

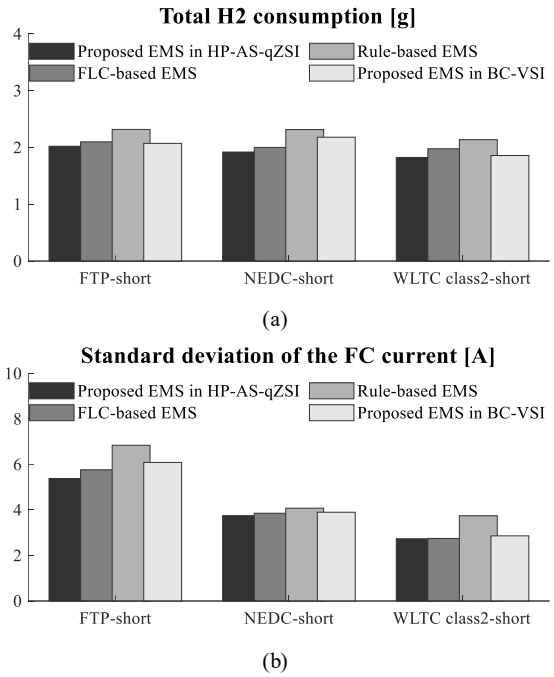

Fig. 16. The experimental results of the FC performance indexes.

V. CONCLUSION

A mode-dependent EMS is implemented to improve the energy performance for a 3-wheel FC-HEV with a HESS FC/LiC configuration using the HP-AS-qZSI. This strategy is primarily constituted by a GMLP classifier-based DMP and a multi-mode FLC. Firstly, four FLCs are realized offline by an IDE algorithm based on the predicted driving modes of the WLTC driving cycle. The DMP recognizes the driving modes and triggers the most suitable FLC at each update to efficiently fulfill the FC power for the vehicle. The performance of the proposed EMS is then compared to offline optimized FLCs under three driving cycles of FTP, NEDC, and WLTC. The reduced-scale HIL is finally executed to verify the effectiveness of the suggested strategy in real-time operation under the investigated driving cycles.

The HIL experimental results have illustrated that the proposed EMS performs a decrease in the H_2 consumption and the standard deviation of the FC current by 12.67% and 21.31%, respectively under the FTP-short driving cycle, compared to the rule-based EMS. These results indicate that the proposed EMS will be a potential framework to improve the energy performance of a three-wheel FC-HEV in terms of the FC hydrogen consumption and current fluctuation. Furthermore, this suggested framework can also be extended to other FC-HEV applications. To further broaden this work, the effect of component sizing on the performance of FC-HEVs based on the dual-source HP-AS-qZSI will be evaluated. Additionally, a detailed model of the GaN device considering its thermal management will be investigated on the real-time simulator to develop the powertrain of the FC-HEV.

REFERENCES

[1] A. Macias Fernandez, M. Kandidayeni, L. Boulon, and J. P. Trovao, "Effects of Price Range Variation on Optimal Sizing and Energy Management Performance of a Hybrid Fuel Cell Vehicle," *IEEE Transactions on Energy Conversion*, vol. 38, no. 3, pp. 1626–1638, Sep. 2023.

[2] M. Kandidayeni, H. Chaoui, L. Boulon, S. Kelouwani, and J. P. F. Trovao, "Online System Identification of a Fuel Cell Stack with Guaranteed Stability for Energy Management Applications," *IEEE Transactions on Energy Conversion*, vol. 36, no. 4, pp. 2714–2723, Dec. 2021.

[3] P. Thounthong, S. Raël, and B. Davat, "Analysis of supercapacitor as second source based on fuel cell power generation," *IEEE Transactions on Energy Conversion*, vol. 24, no. 1, pp. 247–255, 2009.

[4] T. V. Do, M. Kandidayeni, J. P. F. Trovao, and L. Boulon, "Multi-Criteria Ranking of Z-Source Inverter Topologies for a Three-Wheel Fuel Cell Hybrid Electric Vehicle," *IEEE Trans Veh Technol*, pp. 1–11, May 2023.

[5] A. Battiston, J.-P. Martin, E.-H. Miliani, B. Nahid-Mobarakeh, S. Pierfederici, and F. Meibody-Tabar, "Comparison Criteria for Electric Traction System Using Z-Source/Quasi Z-Source Inverter and Conventional Architectures," *IEEE J Emerg Sel Top Power Electron*, vol. 2, no. 3, pp. 467–476, 2014.

[6] T. V. Do, M. Kandidayeni, J. P. F. Trovao, and L. Boulon, "Dual-Source High-Performance Active Switched Quasi-Z-Source Inverter for Fuel Cell Hybrid Vehicles," *IEEE Trans Power Electron*, 2023.

[7] T. V. Do, P. Messier, J. P. Trovao, and L. Boulon, "Three-Wheel Fuel Cell Hybrid Vehicle with a High-Performance Active Switched Quasi-Z-Source Inverter," in *2022 IEEE Vehicle Power and Propulsion Conference, VPPC 2022*, Merced, CA, USA, 2022, pp. 1–6.

[8] H. Hemi, J. Ghouili, and A. Cheriti, "A real time fuzzy logic power management strategy for a fuel cell vehicle," *Energy Convers Manag*, vol. 80, pp. 63–70, Apr. 2014.

[9] A. Tani, M. B. Camara, and B. Dakyo, "Energy management based on frequency approach for hybrid electric vehicle applications: Fuel-cell/lithium-battery and ultracapacitors," *IEEE Trans Veh Technol*, vol. 61, no. 8, pp. 3375–3386, 2012.

[10] W. Zhou, L. Yang, Y. Cai, and T. Ying, "Dynamic programming for new energy vehicles based on their work modes Part II: Fuel cell electric vehicles," *J Power Sources*, vol. 407, pp. 92–104, Dec. 2018.

[11] B. H. Nguyen, T. Vo-Duy, M. C. Ta, and J. P. F. Trovao, "Optimal Energy Management of Hybrid Storage Systems Using an Alternative Approach of Pontryagin's Minimum Principle," *IEEE Transactions on Transportation Electrification*, vol. 7, no. 4, pp. 2224–2237, Dec. 2021.

[12] R. Ghaderi, M. Kandidayeni, M. Soleymani, L. Boulon, and J. P. F. Trovao, "Online Health-Conscious Energy Management Strategy for a Hybrid Multi-Stack Fuel Cell Vehicle Based on Game Theory," *IEEE Trans Veh Technol*, vol. 71, no. 6, pp. 5704–5714, Jun. 2022.

[13] J. Han, D. Kum, and Y. Park, "Synthesis of Predictive Equivalent Consumption Minimization Strategy for Hybrid Electric Vehicles Based on Closed-Form Solution of Optimal Equivalence Factor," *IEEE Trans Veh Technol*, vol. 66, no. 7, pp. 5604–5616, Jul. 2017.

[14] A. Rezaei, J. B. Burl, and B. Zhou, "Estimation of the ECMS Equivalent Factor Bounds for Hybrid Electric Vehicles," *IEEE Transactions on Control Systems Technology*, vol. 26, no. 6, pp. 2198–2205, Nov. 2018.

[15] B. H. Nguyen, R. German, J. P. F. Trovao, and A. Bouscayrol, "Real-time energy management of battery/supercapacitor electric vehicles based on an adaptation of pontryagin's minimum principle," *IEEE Trans Veh Technol*, vol. 68, no. 1, pp. 203–212, Jan. 2019.

[16] K. Ettihir, L. Boulon, and K. Agbossou, "Optimization-based energy management strategy for a fuel cell/battery hybrid power system," *Appl Energy*, vol. 163, pp. 142–153, Feb. 2016.

[17] J. Wu, H. He, J. Peng, Y. Li, and Z. Li, "Continuous reinforcement learning of energy management with deep Q network for a power split hybrid electric bus," *Appl Energy*, vol. 222, pp. 799–811, Jul. 2018.

[18] M. Adnane, B. H. Nguyen, A. Khoumsi, and J. P. F. Trovao, "Driving Mode Predictor-Based Real-Time Energy Management for Dual-Source Electric Vehicle," *IEEE Transactions on Transportation Electrification*, vol. 7, no. 3, pp. 1173–1185, Sep. 2021.

[19] M. Kandidayeni, A. O. Macias Fernandez, A. Khalatbarisoltani, L. Boulon, S. Kelouwani, and H. Chaoui, "An Online Energy Management Strategy for a Fuel Cell/Battery Vehicle Considering the Driving Pattern and Performance Drift Impacts," *IEEE Trans Veh Technol*, vol. 68, no. 12, pp. 11427–11438, Dec. 2019.

[20] J. Cao, H. He, and D. Wei, "Intelligent SOC-consumption allocation of commercial plug-in hybrid electric vehicles in variable scenario," *Appl Energy*, vol. 281, Jan. 2021.

[21] R. Zhang and J. Tao, "GA-Based fuzzy energy management system for FC/SC-Powered HEV Considering H2 Consumption and Load Variation," *IEEE Transactions on Fuzzy Systems*, vol. 26, no. 4, pp. 1833–1843, Aug. 2018.

[22] S. Hu, Z. Liang, and X. He, "Ultracapacitor-Battery Hybrid Energy Storage System Based on the Asymmetric Bidirectional Z-Source Topology for EV," *IEEE Trans Power Electron*, vol. 31, no. 11, pp. 7489–7498, Nov. 2016.

[23] S. Hu, Z. Liang, D. Fan, and X. He, "Hybrid Ultracapacitor-Battery Energy Storage System Based on Quasi-Z-source Topology and Enhanced Frequency Dividing Coordinated Control for EV," *IEEE Trans Power Electron*, vol. 31, no. 11, pp. 7598–7610, Nov. 2016.

[24] L. de Oliveira-Assis *et al.*, "Simplified model of battery energy-stored quasi-Z-source inverter-based photovoltaic power plant with Twofold energy management system," *Energy*, vol. 244, Apr. 2022.

[25] G. Say, S. H. Hosseini, and P. Esmaili, "Hybrid Source Multi-Port Quasi-Z-Source Converter with Fuzzy-Logic-Based Energy Management," *Energies (Basel)*, vol. 16, no. 12, Jun. 2023.

[26] M. Matar and R. Iravani, "FPGA implementation of the power electronic converter model for real-time simulation of electromagnetic transients," *IEEE Transactions on Power Delivery*, vol. 25, no. 2, pp. 852–860, Apr. 2010.

[27] G. Squadrito, G. Maggio, E. Passalacqua, F. Lufrano, and A. Patti, "Empirical equation for polymer electrolyte fuel cell (PEFC) behaviour," *J Appl Electrochem*, vol. 29, no. 12, pp. 1449–1455, 1999.